Supplementary Information

Hidden magnetism and split off flat bands in the insulator metal transition in VO_2

Xiuwen Zhang*, Jia-Xin Xiong & Alex Zunger *

Renewable and Sustainable Energy Institute, University of Colorado, Boulder, Colorado 80309, USA

*e-mail: xiuwen.zhang@colorado.edu; alex.zunger@colorado.edu

1 Electronic structures of nonmagnetic VO_2

The electronic structures of the nonmagnetic monoclinic (M) and rutile (R) phases of VO_2 have been studied by using different types of exchange-correlation functionals [1-6], namely, the local density approximation (LDA) [7], the Perdew-Burke-Ernzerhof (PBE) exchange-correlation functional [8], PBE with on-site electronic Coulomb correlation term *U* [9], the strongly constrained and appropriately normed (SCAN) meta-GGA functional [10], the Heyd-Scuseria-Ernzerhof (HSE) functional [11], and the cluster dynamical mean-field theory (DMFT) [12,13]. Supplementary Table 1 lists the V-V dimerization and band gaps of nonmagnetic monoclinic and rutile VO_2 in preceding theoretical studies [1-6] and the current theoretical study based on the revised PBE exchange-correlation functional (R-PBE) [14] and HSE (α = 0.1). The current R-PBE and HSE (α = 0.1) calculations without *U* employ structural minimization by the corresponding functionals.

Supplementary Fig. 1 shows the first Brillouin zone for the band structure evaluation in Fig. 2a,b for the nonmagnetic M phase. The rutile (in M-like unit cell) and monoclinic structures evaluated in Fig. 2a,b are shown in Supplementary Fig. 2a,b. In the rutile structure (Supplementary Fig. 2a), the V atoms form uniform straight V chains. In the monoclinic structures (Supplementary Fig. 2b), pairs of V atoms in the chain move close to each other to be dimerized with the orientations of V-V dimers deviating from the direction of the V chains (the *a*-axis of the crystal). Supplementary Fig. 3 shows that constraining the orientations of V-V dimers to be along the V chains will not change the insulating band gap significantly (from 0.14 eV in Fig. 2b to 0.15 eV in Supplementary Fig. 3a) while maintaining the split-off flat bands (in bold red), suggesting that the V-V dimerization symmetry breaking induced band gap and split-off flat bands in VO_2 are robust against variations of V-V dimer orientations. However, the change of V-V dimer orientation does change the band dispersion, as shown by Fig. 2b and Supplementary Fig. 3a.

Supplementary Fig. 4 shows the density of states of nonmagnetic monoclinic VO_2 with a degree of bond alternation (DBA) of 26.3% obtained via structural minimization with HSE (α =

0.1), predicting a band gap of 0.66 eV, in agreement with the experimental optical band gap of 0.6-0.7 eV [15].

Supplementary Table 1 Predicted versus assumed degrees of bond alternation and calculated band gaps of nonmagnetic monoclinic and rutile phases of VO_2 based on different types of exchange-correlation functionals in preceding theoretical studies [1-6] and the current theoretical study.

XC functional	Monoclinic: DBA assumed or predicted from energy minimization	Monoclinic: predicted band gap (eV)	Rutile: band gap (eV)
LDA [a]	Predicted 21.9% and used in gap calc.	0	Not reported
PBE [b]	Predicted 14.7% and used in gap calc.	0	0
PBE + *U* (*U* = 3.4 eV) [c]	Predicted 22.5% and used in gap calc.	0.65	0
SCAN [c]	Predicted 24.5% and used in gap calc.	0.32	0
HSE [d]	Assumed 18.9% and used in gap calc.	1.1	Not reported
Cluster DMFT (*U* = 4 eV, *J* = 0.68 eV) based on LDA [e]	Assumed 16.3% and used in gap calc.	0.6	Not reported
Cluster DMFT (*U* = 2.2 eV) based on LDA [f]	Assumed 18.9% and used in gap calc.	0.7	0
R-PBE (current work)	Predicted 25.6% and used in gap calc.	0.14	0
HSE (α = 0.1) (current work)	Predicted 26.3% and used in gap calc.	0.66	0

[a]ref. [1]; [b]ref. [2]; [c]ref. [3]; [d]ref. [4]; [e]ref. [5]; [f]ref. [6]

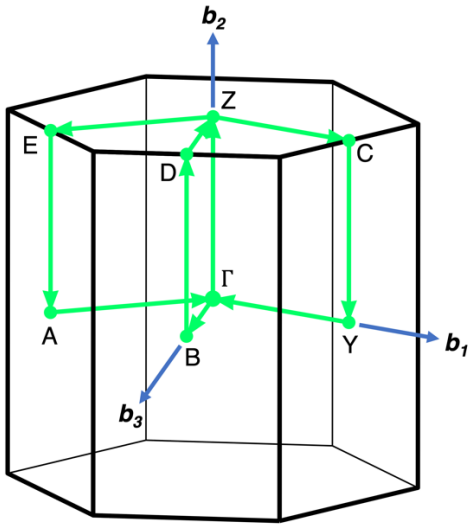

Supplementary Fig. 1 The first Brillouin zone for the monoclinic lattice of VO_2 with marked symmetry points and the *k*-path along which the band structure was calculated.

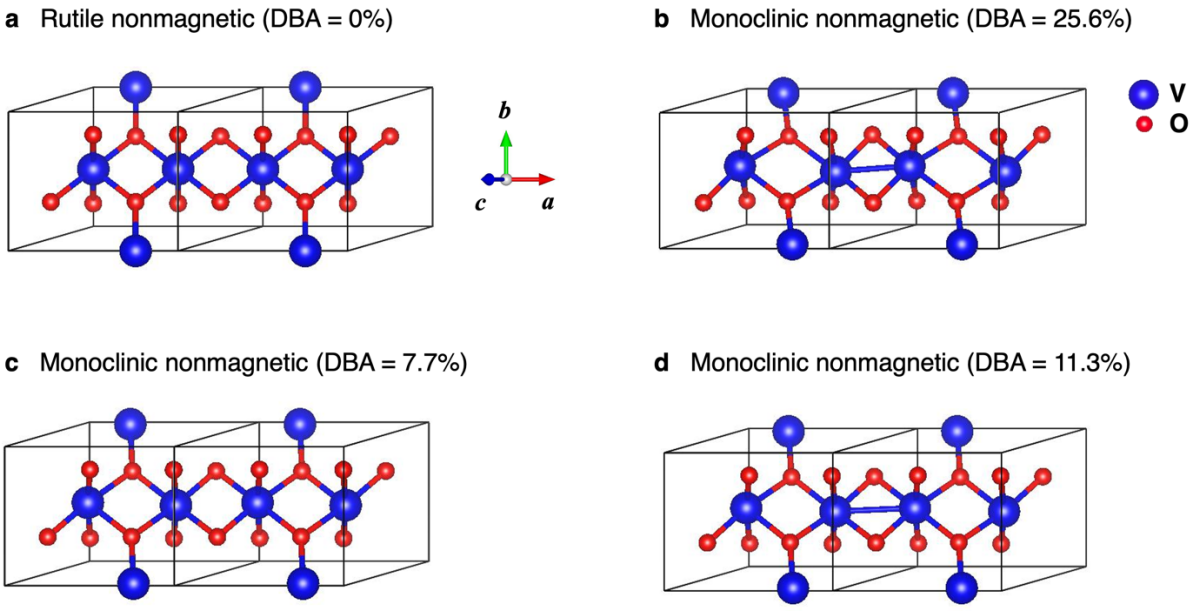

Supplementary Fig. 2 Demonstration of the transition from the rutile to the monoclinic phase of VO_2 in the nudged elastic band calculations of nonmagnetic VO_2 in Fig. 4a. **a** Crystal structure of nonmagnetic rutile VO_2 in the M-like unit cell relaxed by R-PBE. **b** Crystal structure of the nonmagnetic monoclinic VO_2 relaxed by R-PBE. **c**,**d** Crystal structures of the intermediate images of the NEB calculations for the nonmagnetic configuration in Fig. 4a.

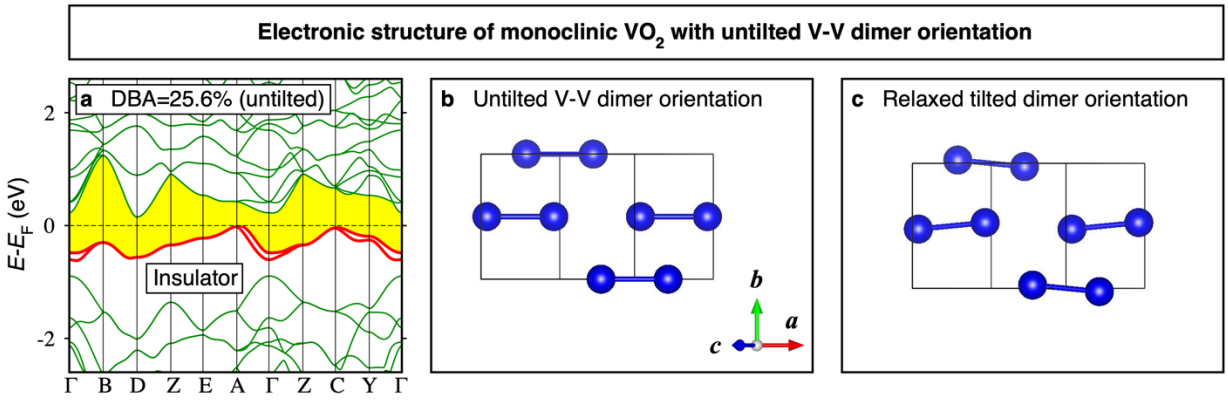

Supplementary Fig. 3 Formation of split-off bands in nonmagnetic monoclinic VO_2 with untilted V-V dimers. a Electronic structure from R-PBE of nonmagnetic monoclinic VO_2 with the same degree of bond alternation as the relaxed monoclinic structure from R-PBE (25.6%), but untilted V-V dimers (aligned along the V chains), as opposed to the tilted V-V dimers in the relaxed structure. **b** Crystal structure of the monoclinic VO_2 showing only the V-V dimers, which is obtained by changing the orientations of the V-V dimers into the direction of the V chains (the *a*-axis of the crystal) in the relaxed monoclinic phase from R-PBE and relaxing the structure internally while keeping the degree of bond alternation (25.6%) and the orientation of the V-V dimers (along the *a*-axis) constrained. **c** Crystal structure of the relaxed monoclinic phase from R-PBE demonstrating only the tilted V-V dimers with orientations different than the direction of the V chains.

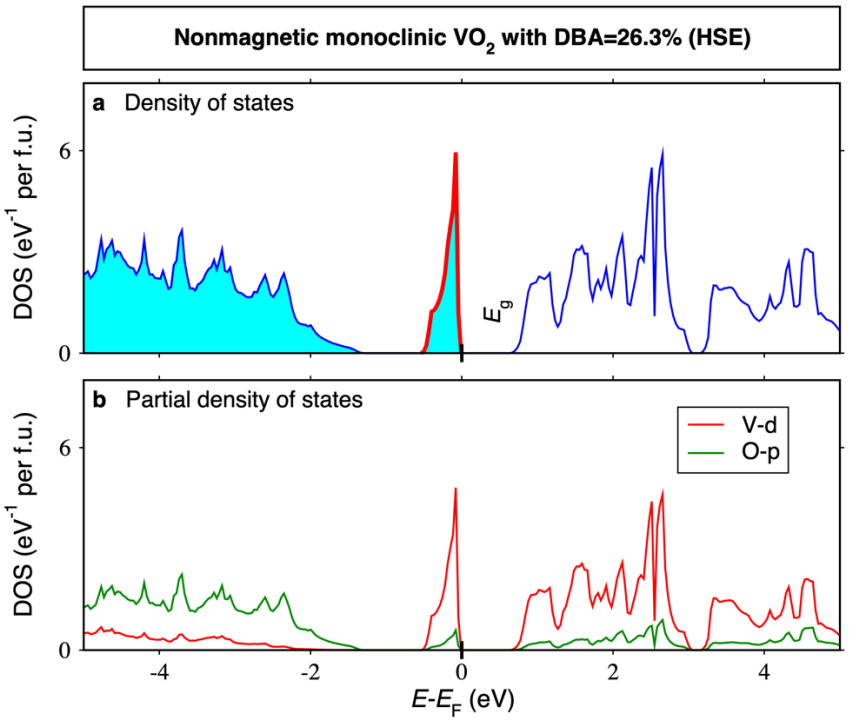

Supplementary Fig. 4 Density of states of nonmagnetic monoclinic VO_2 with degree of bond alternation of 26.3% obtained via structural minimization with HSE. a Total density of states from HSE (α = 0.1). Blue area indicates the occupied states. The split-off flat-band states are indicated by bold red boundary, which have a band width of 0.52 eV and are separated from the other *d* states in the conduction band by 0.66 eV (E_g). **b** Partial density of states.

2 Relaxation of local magnetic moments in the monoclinic phase with large V-V dimerization

The ground state monoclinic phase of VO_2 is believed to be nonmagnetic [1,5,15,16]. We found in our nudged elastic band (NEB) calculations (Fig. 4) with R-PBE that the large V-V dimerization in the M phase of VO_2 suppresses local magnetic moments (Fig. 4b), leading to the nonmagnetic monoclinic phase. Similarly, the long-range ordered magnetic configurations (Mag-1, 2, 3, see Fig. 4a) in the unit cell of monoclinic VO_2 relax into the nonmagnetic configuration (i.e., initial local magnetic moments relax to zero) in HSE (α = 0.1). To further confirm that large V-V dimerization in the M phase suppresses magnetic moments, we construct spin special quasirandom structure (spin-SQS) on the $1 \times 2 \times 2$ supercell (48-atom) of the monoclinic structure and monitor the local magnetic moments during relaxation. Supplementary Fig. 5 shows that the initial spin-SQS magnetic configuration on the supercell of the M structure relax into the nonmagnetic configuration (i.e., initial local magnetic moments relax to zero) after cell-internal relaxation or combined cell-shape and cell-internal relaxations. We notice that ferromagnetic configuration is used in many DFT databases because it is the simplest magnetic configuration, but as found out in ref. [17] that it is a poor representation of paramagnetic phases. For VO_2, the relaxed ferromagnetic configuration of the monoclinic phase is found to be 29 meV per atom (26 meV

per atom) lower-in-energy than the nonmagnetic configuration of the monoclinic phase from R-PBE [HSE (α = 0.1)], although the former has a rather small degree of bond alternation (DBA) of 9.1% (10.1%) and a metallic electronic structure, let alone the macroscopic magnetic moment that was not observed in experiments [18,19]. For comparison, the relaxed ferromagnetic configuration of rutile VO_2 is found to be 29 meV per atom (23 meV per atom) lower-in-energy than nonmagnetic monoclinic VO_2 from R-PBE [HSE (α = 0.1)], although macroscopic magnetic moments were not observed in rutile VO_2 [18,19].

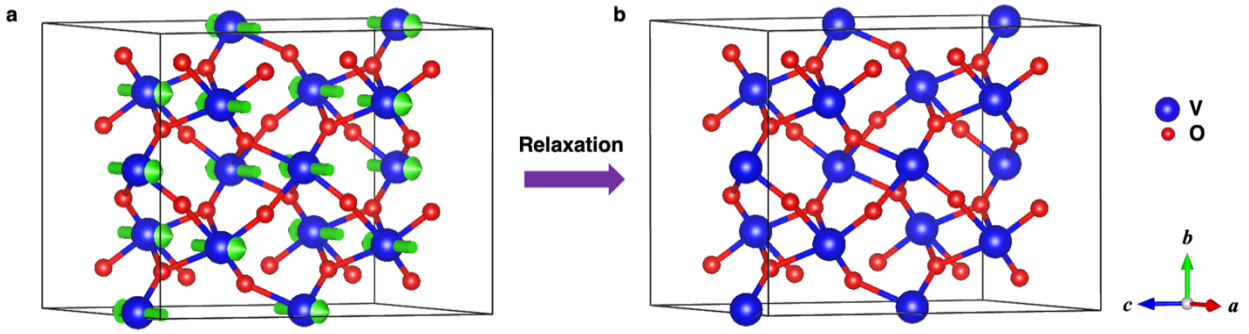

Supplementary Fig. 5 Relaxation of local magnetic moments in monoclinic VO_2 with large V-V dimerization. a Initial paramagnetic configuration of the monoclinic phase with DBA = 25.6%. **b** Final nonmagnetic configuration after cell-internal relaxation or combined cell-shape and cell-internal relaxations with R-PBE. The initial paramagnetic configuration of monoclinic VO_2 is modelled by the spin-SQS structure of the $1 \times 2 \times 2$ supercell (48-atom) of the monoclinic structure relaxed by R-PBE.

3 Structural transitions from the rutile to the monoclinic phase of VO_2

The transition from the R to the M phase of VO_2 along the minimum-energy path of the nudged elastic band calculations of the nonmagnetic configuration (see Fig. 4a) is demonstrated in Supplementary Fig. 2, showing that as the degree of bond alternation increases, pairs of V atoms move close to each other to form dimers. The monoclinic structure with DBA of 11.3% as shown in Supplementary Fig. 2d is the single local-maximal-energy intermediate image in the NEB calculations for the nonmagnetic configuration (see Fig. 4a). The minimum-energy path for Mag-1 (Mag-3) configuration also has a single local-maximal-energy intermediate image at 12.5% (14.1%) (see Supplementary Fig. 6). However, the minimum-energy path for Mag-2 configuration has two local maxima at degrees of bond alternation of 3.4% and 17.9%, respectively (see Fig. 4a and Supplementary Fig. 7). For calculating the phase transition barrier, we use the local maximum at DBA = 3.4% as the intermediate image with maximal energy of 0.034 eV per V-V dimer (higher than the rutile structure). The endpoint monoclinic (rutile) structure of the NEB calculations for the Mag-2 (Mag-1 or Mag-3) configuration is identical with (analogous to) the endpoint monoclinic (rutile) structure for the nonmagnetic configuration. As shown in Supplementary Fig.

2,6,7, the structural transition from the R to the M phase in the NEB calculations for the magnetic configurations (Mag-1,2,3) is analogous to the structural transition in the NEB calculations for nonmagnetic VO_2.

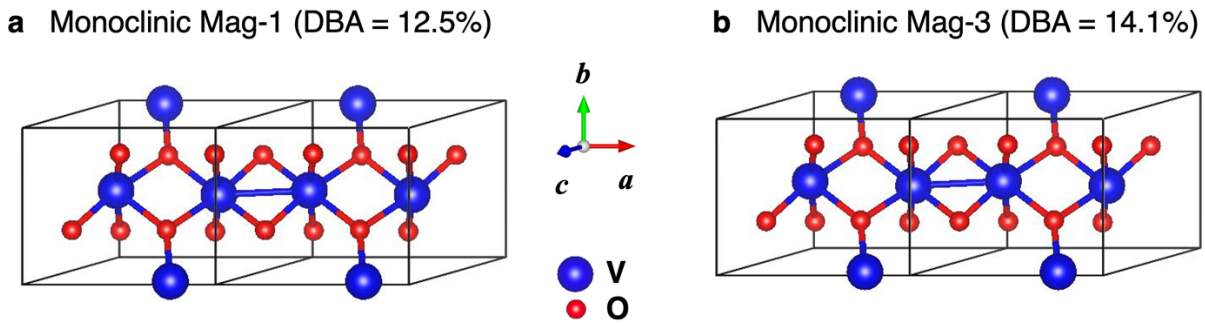

Supplementary Fig. 6 Crystal structures of the intermediate images with the maximal energies in the nudged elastic band calculations of VO_2 in Mag-1 and Mag-3 configurations in Fig. 4a. **a** Crystal structure of the maximal-energy intermediate image for magnetic configuration Mag-1 (see Fig. 4a). **b** Mag-3.

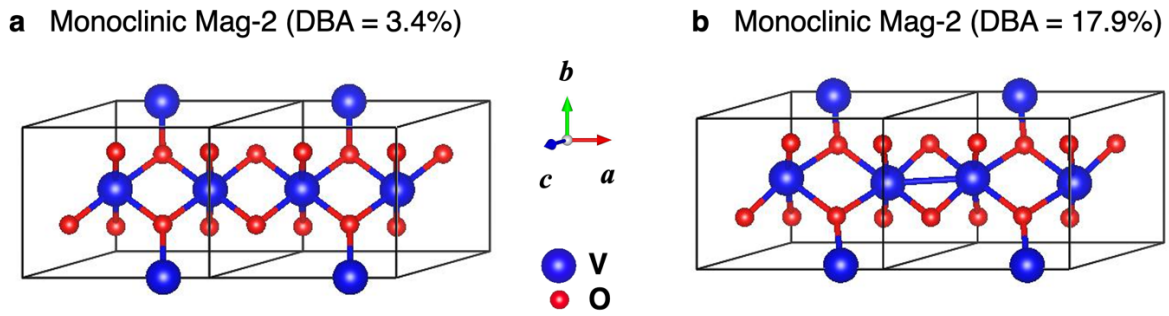

Supplementary Fig. 7 Crystal structures of the intermediate images with the maximal energies in the nudged elastic band calculations of VO_2 in the Mag-2 configuration in Fig. 4a. **a** DBA = 3.4%. **b** DBA = 17.9%.

4 Non-relativistic spin splitting in the magnetic rutile phase

Surprisingly, we observe large spin splitting (for example reaching 0.39 eV in the valence band along M-Γ path) in the magnetic rutile phase of VO_2, with the Mag-2 magnetic configuration as shown in Fig. 4a, which are non-relativistic spin splitting independent of spin-orbit coupling [20]. The magnetic space group $P4_{2'}/mnm'$ fulfills the symmetry requirement for non-relativistic spin splitting [20-22]. The resulted spin splitting is shown in Supplementary Fig. 8.

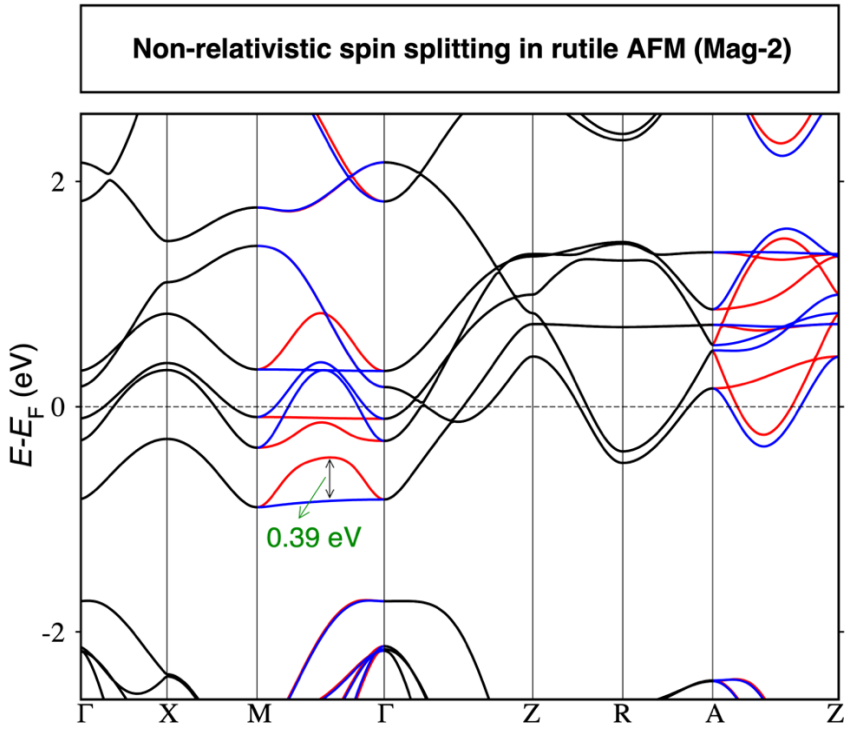

Supplementary Fig. 8 Electronic structure with large spin splitting of rutile VO_2 with the Mag-2 magnetic configuration (see Fig. 4a) from R-PBE. Red (blue) curve: spin up (down). Black curve: spin degenerate.

5 The *d*-bands splitting in monoclinic VO_2

In the monoclinic and rutile phases of VO_2, the crystal field of the VO_6 octahedral splits the V-*d* orbital into t_{2g} and e_g states. The crystal field in monoclinic VO_2 further splits the t_{2g} and e_g states into the a_{1g}, e_g^{π}, and e_g^{σ} states. Supplementary Fig. 9 shows the a_{1g} partial density of states of nonmagnetic monoclinic VO_2, demonstrating the splitting between the occupied bonding $d_{||}$ bands and the unoccupied anti-bonding $d_{||}$ bands.

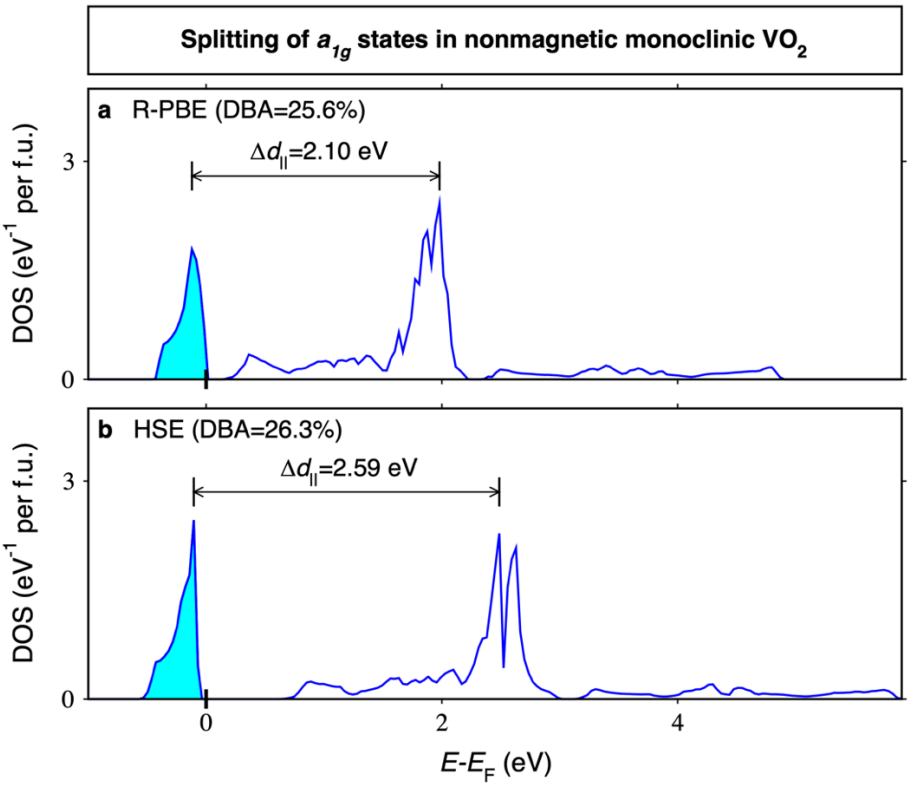

Supplementary Fig. 9 Energy splitting of bonding and anti-bonding $d_{||}$ bands in nonmagnetic monoclinic VO_2. a Partial density of states of nonmagnetic monoclinic VO_2 with DBA = 25.6% obtained via structural minimization from R-PBE, for the bonding $d_{||}$ bands (split-off bands as shown by bold red curves in Fig. 2b) and the anti-bonding $d_{||}$ bands that mainly consist of a_{1g} states. **b** Partial density of states for a_{1g} of nonmagnetic monoclinic VO_2 with DBA = 26.3% obtained via structural minimization from HSE (α = 0.1). Blue area indicates the occupied states.

6 Constrained theoretical calculation for the magnetic monoclinic phase

At ambient conditions, the dynamic variation of V-V dimerization could induce hidden magnetism in the transient monoclinic phases. To investigate the effect of hidden magnetism in the transient phases on the electronic structure of M VO_2, we performed the constrained theoretical calculation for the spin-SQS structure on the $1 \times 2 \times 2$ supercell of the experimental M structure [23] from HSE (α = 0.1) without structural relaxation. Supplementary Fig. 10 shows the partial density of states of the paramagnetic monoclinic phase on a spin-up V ion belonging to a spin parallel V-V dimer, and those on a spin-up V ion belonging to a spin anti-parallel V-V dimer, demonstrating that the spin parallel V-V dimer induces the large band width for the isolated split-off bands (see Fig. 6). Supplementary Fig. 11 illustrates that in the spin parallel V-V dimer, the two a_{1g} states from the two V ions have the same spin and strongly couple with each other, leading to the large band width for the isolated split-off bands, whereas in spin anti-parallel V-V dimer, the two a_{1g} states from the two V ions have opposite spins and no strong coupling.

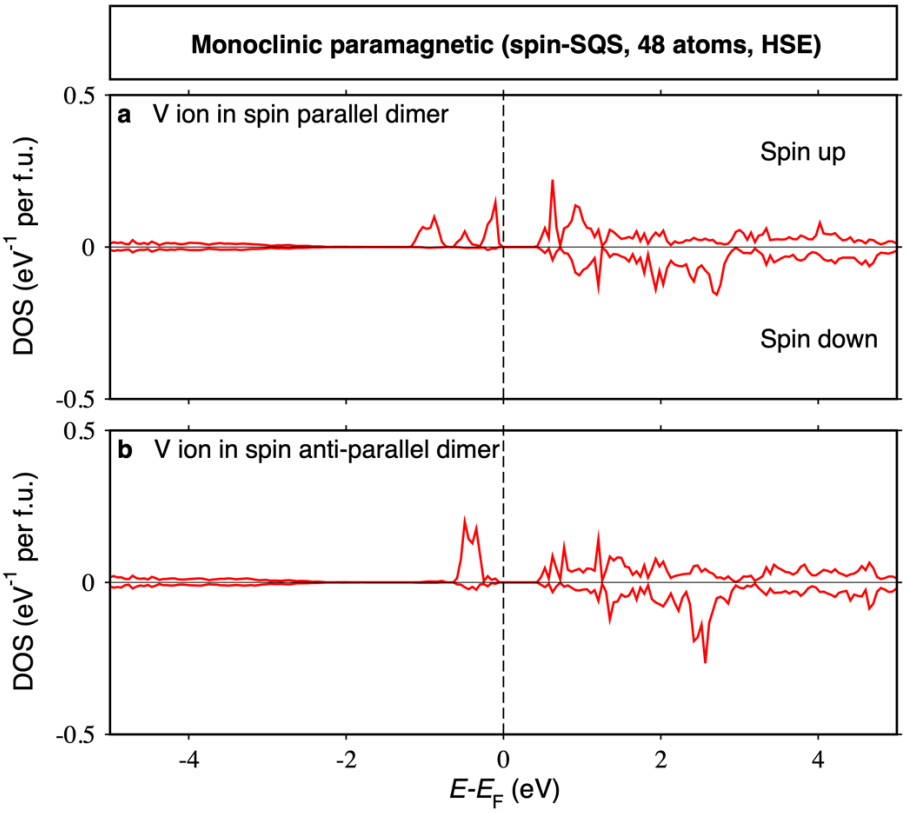

Supplementary Fig. 10 Partial density of states from HSE (α = 0.1) of the fixed experimental monoclinic structure with degree of bond alternation of 18.9%. a V-*d* partial density of states on a spin-up V ion belonging to a spin parallel V-V dimer of the paramagnetic monoclinic phase of VO_2 as modelled by the spin-SQS structure of the $1 \times 2 \times 2$ supercell (48-atom) of the experimental monoclinic structure. **b** V-*d* partial density of states on a spin-up V ion belonging to a spin anti-parallel dimer.

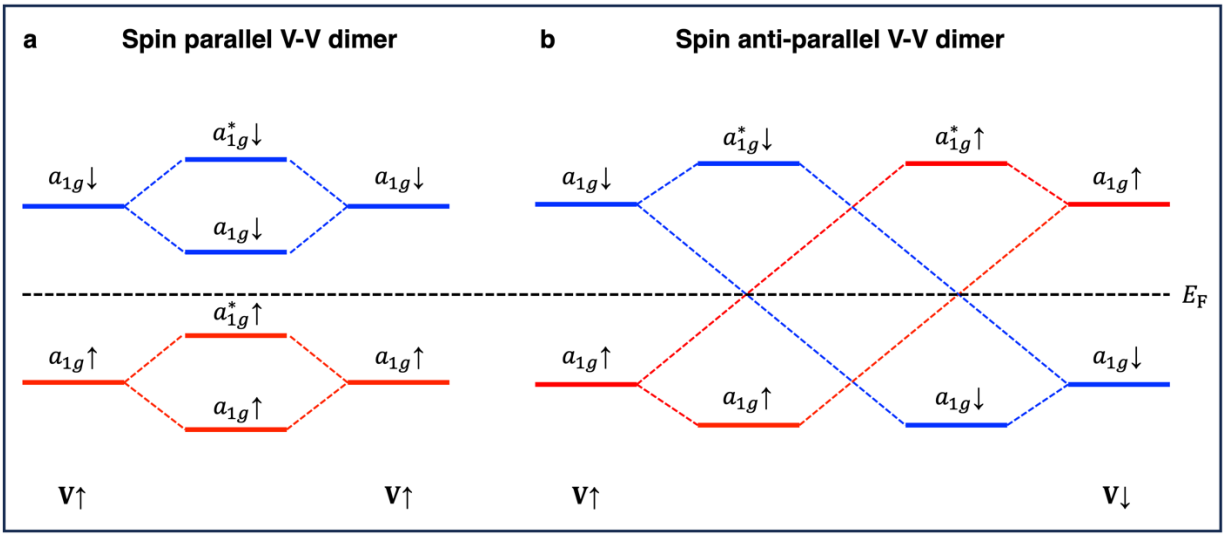

Supplementary Fig. 11 Schematic diagram showing the splitting of the a_{1g} states in the magnetic phase of monoclinic VO_2. a Spin parallel V-V dimer in magnetic monoclinic VO_2. **b** Spin anti-parallel V-V dimer.

REFERENCES

1 Wentzcovitch, R. M., Schulz, W. W. & Allen, P. B. VO2 - Peierls or Mott-Hubbard - a View from Band Theory. *Phys. Rev. Lett.* **72**, 3389-3392 (1994).

2 Mondal, W. R. *et al.* Role of V-V dimers on structural, electronic, magnetic, and vibrational properties of VO2 by first-principles simulations and Raman spectroscopic analysis. *Phys. Rev. B* **103**, 214107 (2021).

3 Stahl, B. & Bredow, T. Critical Assessment of the DFT plus U Approach for the Prediction of Vanadium Dioxide Properties. *J. Comput. Chem.* **41**, 258-265 (2020).

4 Eyert, V. VO2: A Novel View from Band Theory. *Phys. Rev. Lett.* **107**, 016401 (2011).

5 Biermann, S., Poteryaev, A., Lichtenstein, A. I. & Georges, A. Dynamical singlets and correlation-assisted peierls transition in VO2. *Phys. Rev. Lett.* **94**, 026404 (2005).

6 Lazarovits, B., Kim, K., Haule, K. & Kotliar, G. Effects of strain on the electronic structure of VO2. *Phys. Rev. B* **81**, 115117 (2010).

7 Perdew, J. P. & Zunger, A. Self-Interaction Correction to Density-Functional Approximations for Many-Electron Systems. *Phys. Rev. B* **23**, 5048-5079 (1981).

8 Perdew, J. P., Burke, K. & Ernzerhof, M. Generalized gradient approximation made simple. *Phys. Rev. Lett.* **77**, 3865-3868 (1996).

9 Dudarev, S. L., Botton, G. A., Savrasov, S. Y., Humphreys, C. J. & Sutton, A. P. Electron-energy-loss spectra and the structural stability of nickel oxide: An LSDA+U study. *Phys. Rev. B* **57**, 1505-1509 (1998).

10 Sun, J. W., Ruzsinszky, A. & Perdew, J. P. Strongly Constrained and Appropriately Normed Semilocal Density Functional. *Phys. Rev. Lett.* **115**, 036402 (2015).

11 Heyd, J., Scuseria, G. E. & Ernzerhof, M. Erratum: "Hybrid functionals based on a screened Coulomb potential" [J. Chem. Phys. 118, 8207 (2003)]. *J. Chem. Phys.* **124**, 219906 (2006).
12 Lichtenstein, A. I. & Katsnelson, M. I. Antiferromagnetism and d-wave superconductivity in cuprates: A cluster dynamical mean-field theory. *Phys. Rev. B* **62**, R9283-R9286 (2000).
13 Kotliar, G., Savrasov, S. Y., Pálsson, G. & Biroli, G. Cellular dynamical mean field approach to strongly correlated systems. *Phys. Rev. Lett.* **87**, 186401 (2001).
14 Hammer, B., Hansen, L. B. & Norskov, J. K. Improved adsorption energetics within density-functional theory using revised Perdew-Burke-Ernzerhof functionals. *Phys. Rev. B* **59**, 7413-7421 (1999).
15 Berglund, C. N. & Guggenheim, H. J. Electronic Properties of VO2 near Semiconductor-Metal Transition. *Phys. Rev.* **185**, 1022-1033 (1969).
16 Goodenough, J. B. Direct Cation--Cation Interactions in Several Oxides. *Phys. Rev.* **117**, 1442-1451 (1960).
17 Varignon, J., Bibes, M. & Zunger, A. Origin of band gaps in 3d perovskite oxides. *Nat. Commun.* **10**, 1658 (2019).
18 Yin, C. Y. *et al.* Unusual magnetic transition near metal-insulator transition and paramagnetic anomaly in VO2. *Appl. Phys. Lett.* **110**, 172404 (2017).
19 Zhang, R. *et al.* Understanding of metal-insulator transition in VO2 based on experimental and theoretical investigations of magnetic features. *Sci. Rep.* **8**, 17093 (2018).
20 Yuan, L. D., Wang, Z., Luo, J. W., Rashba, E. I. & Zunger, A. Giant momentum-dependent spin splitting in centrosymmetric low-Z antiferromagnets. *Phys. Rev. B* **102**, 014422 (2020).
21 Yuan, L. D., Wang, Z., Luo, J. W. & Zunger, A. Prediction of low-Z collinear and noncollinear antiferromagnetic compounds having momentum-dependent spin splitting even without spin-orbit coupling. *Phys. Rev. Mater.* **5**, 014409 (2021).
22 Yuan, L. D. & Zunger, A. Degeneracy Removal of Spin Bands in Collinear Antiferromagnets with Non-Interconvertible Spin-Structure Motif Pair. *Adv. Mater.* **35**, 2211966 (2023).
23 Longo, J. M. & Kierkegaard, P. A Refinement of the Structure of VO2. *Acta Chemica Scandinavica* **24**, 420-426 (1970).